Parametrization of low-energy cross sections for nonresonant neutron capture

Chengbin Wang,[1,*] Ousmane I. Cissé,[2,†] and Daniel Baye[3,‡]

[1]*Shanghai Institute of Applied Physics, Chinese Academy of Science, Shanghai 201800, People's Republic of China*

[2]*UFR SEA, Département de Physique, Université de Ouagadougou, 03 BP 7021 Ouagadougou 03, Burkina Faso*

[3]*Physique Quantique, C. P. 165/82, and Physique Nucléaire Théorique et Physique Mathématique, C. P. 229, Université Libre de Bruxelles, B-1050 Brussels, Belgium*

(Received 28 July 2009; published 18 September 2009)

The nonresonant component of radiative neutron capture reactions is parametrized at low energies by a polynomial of second degree. The potential model is first used to reproduce experimental data below 1 MeV with the help of spectroscopic factors. The fits are found sensitive to the scattering length of the initial s or p waves. The coefficients of a Taylor expansion are then calculated by resolution of the Schrödinger equation and its energy derivatives at energy zero. Such theory-guided parametrizations are derived for neutron capture by ^{7}Li, ^{12}C, ^{14}C, ^{16}O, and ^{18}O. When the capture proceeds from the s wave to a weakly bound state, a Padé-like parametrization better approximates the potential-model results.

DOI: 10.1103/PhysRevC.80.034611 PACS number(s): 25.40.Lw, 27.20.+n, 28.20.Ka, 24.50.+g

I. INTRODUCTION

Many capture cross sections are measured accurately for thermal neutrons. However, in the keV to MeV domain, fewer experiments are available, and their difficulty often leads to rather large error bars [1–12]. Moreover, the occurrence of resonances can even complicate the interpretation of data. It is thus difficult to extract simple and precise expressions giving direct capture cross sections below about 1 MeV. Simple parametrizations of these cross sections over a low-energy domain would be very useful to interpolating these data. They can also help in deriving the properties of low-energy resonances from deviations with respect to such parametrizations.

The derivation of a simple though precise parametrization is easier when it is guided by theoretical considerations. Indeed, the nonresonant behavior of low-energy capture cross sections is well established theoretically. The purpose of this work is to perform such analyses for several cases where enough data exist. At low energies, a neutron capture cross section $\sigma(E)$ to a given bound state can be approximated at relative energy E by a Taylor expansion truncated at order 2 [13],

$$\sigma v = S_0 E^{l_i}(1 + s_1 E + s_2 E^2), \tag{1}$$

where v is the initial relative velocity and l_i is the smallest relevant orbital momentum of the initial scattering state. The coefficients S_0, s_1, and s_2 of this Taylor expansion can be derived by a simple direct calculation at energy zero in any capture model [13,14]. Notice that S_0 as defined here is slightly different from the definition in Ref. [13] [see Eq. (3) below]. This derivation is particularly simple in the potential model. The coefficients are calculated from the wave function at zero energy and from its energy derivatives which can be obtained from inhomogeneous equations obtained at zero energy by differentiating the Schrödinger equation with respect to energy.

The goal of the present work is to use the simple potential model including spectroscopic factors to provide polynomial approximations of neutron capture cross sections at low energies by various light nuclei for which some data exist. Since the potential model has a limited predictive power, the existence of data is essential to validating the different approximations performed.

The principle of the derivation of the parametrizations is summarized in Sec. II. Polynomial parametrizations are derived for ^{7}Li, ^{12}C, ^{14}C, ^{16}O, ^{18}O in Sec. III. Concluding remarks are presented in Sec. IV.

II. EXPANSION OF CAPTURE CROSS SECTIONS AT LOW ENERGIES

In this section we summarize the technique of calculating the truncated Taylor expansion (1) developed in Ref. [13]. We refer the reader to that reference for details.

A nucleus with mass M and charge Ze captures a neutron with mass m_n at energy E in the center-of-mass frame by an electric transition $E\lambda$ of multipolarity λ. In the potential model, bound and scattering states are described for a given orbital momentum l by the Hamiltonian

$$H_l = -\frac{\hbar^2}{2\mu}\left[\frac{d^2}{dr^2} - \frac{l(l+1)}{r^2}\right] + V(r), \tag{2}$$

where $\mu = m_n M/(M + m_n)$ is the reduced mass of the system and V is a neutron-nucleus interaction which may depend on the considered partial wave. In the LS coupling scheme, a bound state at negative energy E_B is characterized by quantum numbers $l_f J_f$ and a scattering partial wave by quantum numbers $l_i J_i$.

Let us denote as σ the partial cross section for the neutron capture with those specific quantum numbers. The limit of σv for $E \to 0$ is given by

$$S_0 = \alpha c N_{\mathrm{E}\lambda}(|E_B|/\hbar c)^{2\lambda+1}(2\mu/\hbar^2)^{l_i}[I(0)]^2, \tag{3}$$

*mail.chengbinwang@gmail.com
†oicisse@univ-ouaga.bf
‡dbaye@ulb.ac.be

where α is the fine structure constant and c is the speed of light in the vacuum. Coefficient S_0 differs from $\mathcal{S}_0$ of Ref. [13] by a factor of $(2\mu/\hbar^2)^{l_i}$. The constant $N_{\mathrm{E}\lambda}$ reads

$$N_{\mathrm{E}\lambda} = 8\pi Z^2 \left(\frac{m_n}{M}\right)^{2\lambda} \times \frac{(\lambda+1)(2\lambda+1)}{\lambda(2\lambda+1)!!^2} \frac{(2J_i+1)(2J_f+1)(2l_i+1)(2l_f+1)}{2(2I_1+1)} \times \begin{pmatrix} l_f & \lambda & l_i \\ 0 & 0 & 0 \end{pmatrix}^2 \begin{Bmatrix} J_f & l_f & I \\ l_i & J_i & \lambda \end{Bmatrix}^2. \quad (4)$$

The integral $I(0)$ is the limit at zero energy of the usual radial integral $I(E)$ of the potential model. It is given by

$$I(0) = \int_0^\infty u_{l_f}(r) r^\lambda u_{l_i}^0(r) dr, \quad (5)$$

where u_{l_f} is the bound-state wave function solution of the radial Schrödinger equation $H_{l_f} u_{l_f} = E_B u_{l_f}$, and $u_l^0(r)$ is a solution vanishing at the origin of the radial Schrödinger equation at energy 0,

$$H_l u_l^0 = 0. \quad (6)$$

Here and elsewhere, the superscript 0 indicates a limit at energy zero. Since Eq. (6) does not fix the normalization, function u_l^0 must be normalized by imposing the condition

$$W\{\mathcal{G}_l^0, u_l^0\} \underset{r\to\infty}{\longrightarrow} 1, \quad (7)$$

where the Wronskian $W\{g,f\}$ is equal to $g(df/dr) - f(dg/dr)$ and

$$\mathcal{G}_0^0 = 1, \quad \mathcal{G}_1^0 = r^{-1}, \quad \mathcal{G}_2^0 = 3r^{-2}, \ldots \quad (8)$$

The scattering lengths are given by

$$a_l = \frac{2\mu}{\hbar^2} \int_0^\infty \mathcal{F}_l^0(r) V(r) u_l^0(r)\, dr, \quad (9)$$

where

$$\mathcal{F}_0^0 = r, \quad \mathcal{F}_1^0 = \frac{r^2}{3}, \quad \mathcal{F}_2^0 = \frac{r^3}{15}, \ldots \quad (10)$$

The dimensions of the scattering lengths are fm^{2l+1}. General expressions for $\mathcal{F}_l^0$ and $\mathcal{G}_l^0$ can be found in Ref. [13].

The coefficient s_1 in expansion (1) reads

$$s_1 = \frac{2\lambda+1}{|E_B|} + \frac{2I'(0)}{I(0)} - \delta_{l_i 0} \frac{2\mu a_0^2}{\hbar^2}, \quad (11)$$

where a_0 is the s-wave scattering length. The prime indicates a derivative with respect to energy. The integral $I'(0)$ is given by

$$I'(0) = \int_0^\infty u_{l_f}(r) r^\lambda u_{l_i}'^0(r) dr. \quad (12)$$

In this expression, the energy derivative of the radial wave function at zero energy $u_l'^0$ is a solution of the derivative of the Schrödinger equation at the limit $E \to 0$, i.e.,

$$H_l u_l'^0 = u_l^0. \quad (13)$$

Since solutions vanishing at the origin are not uniquely fixed by this equation, one imposes the condition

$$W\{\mathcal{G}_l^0, u_l'^0 - (\mu/\hbar^2)(\mathcal{F}_l'^0 + a_l \mathcal{G}_l'^0)\} \underset{r\to\infty}{\longrightarrow} 0, \quad (14)$$

where a_l is the scattering length of partial wave l and

$$\mathcal{F}_0'^0 = -r^3/3, \quad \mathcal{F}_1'^0 = -r^4/15, \quad \mathcal{F}_2'^0 = -r^5/105, \ldots$$
$$\mathcal{G}_0'^0 = -r^2, \quad \mathcal{G}_1'^0 = r, \quad \mathcal{G}_2'^0 = 1, \ldots \quad (15)$$

The notation f'^0 represents the energy derivative of f calculated at $E = 0$. General expressions for $\mathcal{F}_l'^0$ and $\mathcal{G}_l'^0$ can be found in Ref. [13]. Coefficient s_2 can be calculated in a similar way (see Ref. [13]).

To determine the cross section, we have to choose a potential. To keep the calculations simple, we take the standard Saxon-Woods form

$$V(r) = -\frac{V_{lJ}}{1+\exp[(r-R)/a]}, \quad (16)$$

where coefficient V_{lJ} is adjusted individually for each bound or scattering state. It depends on the quantum numbers l and/or J relevant to the considered state. It may sometimes also depend on the channel spin I. For a bound state, this coefficient is adjusted by fitting its energy. For a scattering state, different strategies will be used depending on the available information. Then, spectroscopic factors $\mathcal{S}_{l_f J_f}$ are introduced with the aim of correcting the simplicity of the bound-state description in the potential model. The partial cross sections are multiplied by these factors to give

$$\sigma = \sum_{l_f J_f} \mathcal{S}_{l_f J_f} \sum_{l_i J_i} \sigma_{l_i J_i \to l_f J_f}, \quad (17)$$

where the sum runs over the considered initial waves and final bound states. Only the $E1$ multipolarity is used in practice here.

We use c.m. energies everywhere. Units are MeV and fm. Coefficients s_1 and s_2 are thus given in MeV^{-1} and MeV^{-2}, respectively. The product σv and coefficient S_0 will be expressed in mb c.

III. PARAMETRIZATIONS OF CROSS SECTIONS

A. Reaction ^{7}Li$(n,\gamma)^8$Li

The 2^+ ground state of ^{8}Li is located at -2.033 MeV with respect to the $^7\mathrm{Li}+n$ threshold. The 1^+ excited state is at -1.052 MeV. A 3^+ resonance occurs near 0.23 MeV.

The $^7\mathrm{Li}(n,\gamma)^8\mathrm{Li}$ has been the subject of a number of experiments in several energy domains. The thermal cross section is 45.4 ± 3 mb [15]. Possible deviations with respect to the $1/v$ low-energy behavior have been searched for from 1.5 to 1340 eV [16]. Further measurements concern the domain 20–600 keV [1,2,5,6,11].

To fit the low-energy experimental data, we use $R = 2.30$ fm and $a = 0.27$ fm [17]. The potential depth for the final bound state is adjusted to reproduce its energy. The obtained depths are given in Table I. The accuracy on V_{lJ} is limited to 0.01 MeV, so the energies may differ slightly from the experimental values throughout this paper. These differences

TABLE I. Energies and potential depths (in MeV) for ^{8}Li.

J^π	l	E	V_{lJ}
2^+	1	−2.034	50.64
1^+	1	−1.048	48.35

have no influence on the accuracy of the parametrizations. The depths for the $l = 0$ scattering states are adjusted to fit the s-wave scattering lengths of the different channel spins: 0.87 ± 0.07 fm for $I = 1$ and -3.63 ± 0.05 fm for $I = 2$ [18]. These scattering lengths are reproduced with the depths 71.80 and 85.36 MeV, respectively. For the d wave, the depth is rather arbitrarily chosen as their average of 78.58 MeV since we have no data to fit. The results for the small d-wave capture component are almost insensitive to this choice.

To provide a parametrization of the nonresonant cross section, we calculate the coefficients of the Taylor expansion with Eqs. (3) and (11). They are displayed in Table II. The spectroscopic factors are taken from Barker [19] and given in the last column of Table II. Choosing other sets of spectroscopic factors [20–22] has little influence on the shape of the results.

The product σv calculated with Eq. (17) as a function of energy E within the potential model and the spectroscopic factors of Table II is displayed in Fig. 1. One observes that the agreement is quite good for the thermal cross section. The data of Blackmon *et al.* [16] represented as triangles correspond to the neutron capture to the ground state. They can be compared with the ground-state capture in the potential model. At low energies, we obtain $\sigma v = 3.0 \times 10^{-4}$ (dash-dotted line). There is a small but systematic discrepancy between the calculated cross sections and the data of Ref. [16], which are on the average located about 10% lower. Higher energy data display the 3^+ resonance. The present nonresonant cross section seems to agree below and above this resonance.

A parametrization of the potential model results is then obtained by weighting the different expressions of Table II with the corresponding spectroscopic factors. The d-wave capture contributes only at order E^2 according to Eq. (1). The experimental data can thus be parametrized as

$$\sigma v = 3.3 \times 10^{-4}(1 - 1.37E + 1.95E^2)\,\mathrm{mb}\,c. \qquad (18)$$

TABLE II. Coefficients S_0, s_1, and s_2 of the Taylor expansions for different transitions of reaction ^{7}Li$(n,\gamma)^8$Li; spectroscopic factors $\mathcal{S}_{lIJ}$.

$J_f^{\pi_f}$	l_i	I	s_1	s_2	S_0	$\mathcal{S}_{lIJ}$
2^+	0	1	−0.165	0.086	1.16×10^{-4}	0.251
		2	−1.492	1.928	3.56×10^{-4}	0.765
	2	1,2	−0.447	0.230	3.97×10^{-5}	1.016
1^+	0	1	−0.285	0.239	3.31×10^{-5}	0.159
		2	−1.698	2.424	8.07×10^{-5}	0.295
	2	1,2	−0.832	0.410	3.59×10^{-5}	0.454

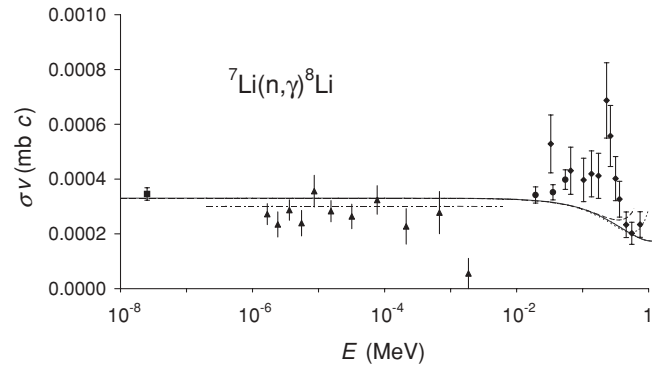

FIG. 1. Comparison of potential model results (full line) and experimental data from Refs. [15] (square), [6] (circles), and [1] (diamonds) for the ^{7}Li$(n,\gamma)^8$Li reaction as a function of neutron c.m. energies in MeV. The ground-state capture is represented as a dash-dotted line and compared with the ^{7}Li$(n,\gamma_0)^8$Li data of Ref. [16] (triangles). Parametrization (18) is represented as a dashed line. The semiempirical parametrization with s_2 replaced by 1.25 is represented as a dotted line.

This parametrization is displayed as a dashed line in Fig. 1. It approximates the potential model up to about 0.2 MeV.

This range is more limited than in most of the cases discussed below. In the present case, the Taylor expansion does not converge well as shown by the large value of s_2. The Padé-like approximations discussed in Sec. III E do not enlarge the domain of validity significantly. However, a good semiempirical parametrization is obtained by replacing coefficient $s_2 = 1.95$ in Eq. (18) by 1.25. The modified second-order polynomial (dotted line in Fig. 1) follows closely the full line up to about 0.6 MeV. This fit is slightly less good than the truncated Taylor expansion around 0.1 MeV.

B. Reaction ^{12}C$(n,\gamma)^{13}$C

This reaction has been studied in detail in Ref. [13]. Here we just adapt the obtained parametrization to the present notation and units,

$$\sigma v = 2.6 \times 10^{-5}(1 + 88E - 50E^2)\,\mathrm{mb}\,c. \qquad (19)$$

It provides a good fit of the data displayed in Fig. 5 of Ref. [13].

C. Reaction ^{14}C$(n,\gamma)^{15}$C

The ^{15}C nucleus possesses only two bound states: $1/2^+$ at −1.218 MeV and $5/2^+$ at −0.478 MeV with respect to the ^{14}C + n threshold. The experimental ^{14}C$(n,\gamma)^{15}$C cross sections have long been controversial [23]. Recent direct measurements performed at neutron energies between 20 and 800 keV [12] now agree with indirect measurements from Coulomb breakup [24]. The thermal cross section is not known. An upper bound is 1 μb.

The potential parameters we use for reaction ^{14}C$(n,\gamma)^{15}$C are taken from Ref. [25]: $R = 2.96$ fm and $a = 0.6$ fm. However, here, we keep the simple form (18) without the spin-orbit term. The depths fitting the bound-state energies are given in Table III. These depths are also used for scattering

TABLE III. Same as Table I, but for ^{15}C.

J^π	l	E	V_{lJ}
$1/2^+$	0	−1.220	52.814
$5/2^+$	2	−0.476	55.98

states in the corresponding partial wave. For the p wave, we take 51.3 MeV, as in Ref. [25].

Since the ground and first excited states of ^{14}C both have a strong single-particle character, their spectroscopic factors can be approximated as 1.0 in the present context. The $E1$ capture to the positive-parity ground and first excited states proceeds from the p wave. The coefficients S_0, s_1, and s_2 calculated as explained in Sec. II are displayed in Table IV. The total product σv decreases with decreasing energy (see Fig. 2). The thermal cross section is due either to an $M1$ transition from the s wave to the $1/2^+$ ground state or to an $E2$ transition from the s wave to the $5/2^+$ bound state. We cannot estimate the $M1$ transitions: they vanish in the present model because of the orthogonality between the initial and final radial wave functions which belong to the same partial wave. We have calculated the $E2$ capture, but it represents less than 10 % of the cross section at thermal energy.

Weighting the various expressions (1) with the spectroscopic factor, the experimental data can thus be parametrized as

$$\sigma v = 1.76 \times 10^{-3} E(1 - 0.85E + 0.54E^2)\,\mathrm{mb}\,c. \quad (20)$$

Notice the additional factor E due to the initial p wave. This simple parametrization is represented by a dashed line in Fig. 2. It is valid up to about 0.8 MeV.

D. Reaction ^{16}O$(n,\gamma)^{17}$O

The ^{17}O nucleus possesses four bound states: $5/2^+$ at −4.144 MeV, $1/2^+$ at −3.273 MeV, $1/2^-$ at −1.088 MeV, and $5/2^-$ at −0.303 MeV with respect to the ^{16}O + n threshold. It also displays a narrow $3/2^-$ resonance near 0.41 MeV. The ^{16}O$(n,\gamma)^{17}$O thermal cross section has been measured as 202 ± 28 μb [26] and 187 ± 10 μb [27]. The branching ratios are (18 ± 3)% to the $1/2^+$ state and (82 ± 3)% to the $1/2^-$ state. Since transitions to the $5/2^-$ state are not observed, we do not consider that state (which is not a single-particle state) in the capture calculation. Measurements have also been performed at neutron energies between 20 and 80 keV [3], at 280 keV [9], and on resonance at 45 keV [9,10].

The potential parameters we use for the reaction ^{16}O$(n,\gamma)^{17}$O are $R = 3.15$ fm and $a = 0.62$ fm. The depths fitting the bound-state energies are given in Table V. For the scattering s wave, we use the depth given in this table. It provides a reasonable scattering length of 5.52 fm. Existing data do not allow us to choose the depth of the scattering p wave. We shall thus use three different depths: 53.6, 60, and 64 MeV corresponding to the p-wave scattering lengths of −10.8, −29.2, and −51.5 fm^3.

The coefficients of the Taylor expansions are given in Table VI for the potential depth 60 MeV in the initial p wave. Since the ground state and the first excited state of ^{17}O both have a strong single-particle character, their spectroscopic factor can be assumed to be 1.0. The second excited state of ^{17}O is not a single-particle state. If we assume that the neutron is in a $p1/2$ wave, the fact that it is not a single-particle state is confirmed by the large depth necessary to reproduce its binding energy. Since the spectroscopic factor of this state is not available, we will fit it on the thermal cross section as explained below.

The $E1$ capture to the positive-parity ground and first excited states proceeds from the p wave. The product σv decreases with decreasing energy, and this behavior cannot explain the order of magnitude of the thermal cross section. Yamamoto *et al.* [28] have proposed to explain the thermal cross section by $M1$ transitions to the $1/2^+$ bound state. However, the experimental branching ratios indicate that thermal transitions mainly lead to the $1/2^-$ bound state. Moreover $M1$ transitions vanish in the present model as explained above. They can be evaluated in a microscopic cluster model [29]. Therefore, we approximate the thermal cross section with an $E1$ transition to the $1/2^-$ state and adjust the spectroscopic factor to the experimental value.

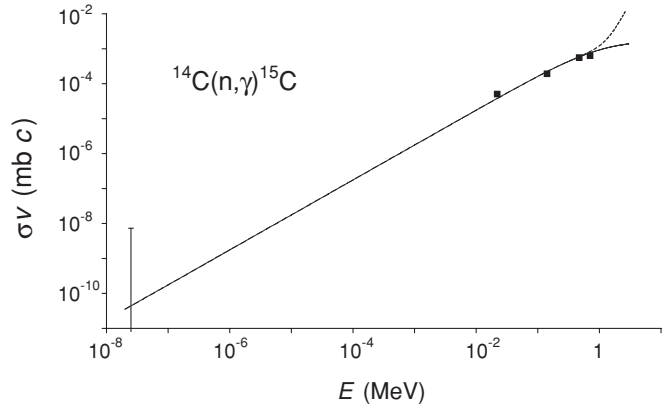

FIG. 2. Comparison of potential model results (full line) and experimental data from Ref. [12] (squares) for the ^{14}C$(n,\gamma)^{15}$C reaction as a function of the neutron c.m. energy in MeV. An upper bound is shown at the thermal energy. Parametrization (20) is represented as a dashed line.

TABLE IV. Same as Table II, but for the reaction ^{14}C$(n,\gamma)^{15}$C.

$J_f^{\pi_f}$	l_f	l_i	s_1	s_2	S_0	$\mathcal{S}_{lJ}$
$1/2^+$	0	1	−0.903	0.654	1.70×10^{-3}	1
$5/2^+$	2	1	0.633	−2.579	6.21×10^{-5}	1

TABLE V. Same as Table I, but for ^{17}O.

J^π	l	E	V_{lJ}
$5/2^+$	2	−4.142	57.26
$1/2^+$	0	−3.274	53.60
$1/2^-$	1	−1.088	78.32

TABLE VI. Same as Table II, but for the reaction $^{16}O(n,\gamma)^{17}O$.

$J_f^{\pi_f}$	l_f	l_i	s_1	s_2	S_0	$\mathcal{S}_{lJ}$
$5/2^+$	2	1	0.516	−0.058	1.73×10^{-3}	1
$3/2^+$	2	1	0.250	−0.124	4.99×10^{-3}	1
$1/2^-$	1	0	0.008	0.060	9.61×10^{-5}	0.015

This approximate procedure leads to a value of 0.015 for the coefficient, which is not strictly a spectroscopic factor since it also simulates the $M1$ transition. The results displayed as a full line in Fig. 3 fairly reproduce the data.

The coefficients S_0, s_1, and s_2 are displayed in Table VI. By weighting the various expressions (1) with the spectroscopic factors, the experimental data can be parametrized as

$$\sigma v = 1.44 \times 10^{-6}(1 + 4660E + 1480E^2)\,\mathrm{mb}\,c. \quad (21)$$

This simple parametrization is represented by a dashed line in Fig. 3. It is valid up to about 1 MeV.

If we use the other depths for the potential of the initial p wave, the agreement of the potential model with the data is less good. Figure 3 shows the corresponding parametrizations as dotted lines. For the smaller depth 53.6 MeV, they lead to smaller capture cross sections, while for the larger depth 64 MeV, they lead to larger ones. The model cross section is thus sensitive to the scattering length of the initial wave. To our knowledge, the p-wave scattering length is not known for such a system. Here we find that it should be negative and lie between −20 and −30 fm^3. This result disagrees with the value found with the microscopic cluster model, which is positive, near 9 fm^3 [30]. It would be interesting to determine the scattering length for which this microscopic model reproduces the capture cross section.

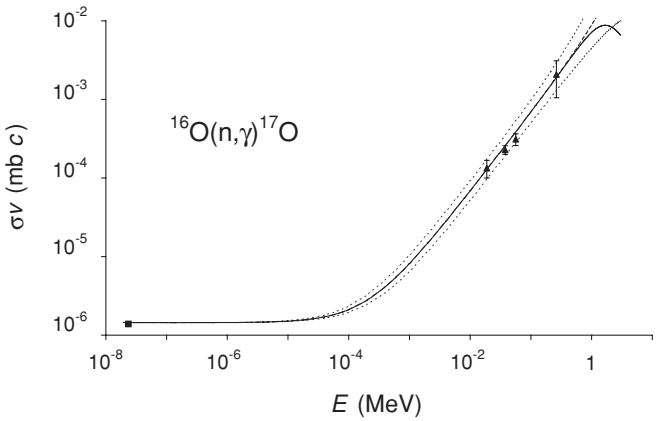

FIG. 3. Comparison of potential model results (full line) and experimental data from Refs. [26,27] (square) and [3] (triangles) for the $^{16}O(n,\gamma)^{17}O$ reaction as a function of the neutron c.m. energy in MeV. The dashed line represents the Taylor expansion (21) for a p-wave scattering length of −29.2 fm^3. The lower and upper dotted lines correspond to p-wave scattering lengths of −10.8 and −51.5 fm^3, respectively.

TABLE VII. Same as Table I, but for ^{19}O.

J^π	l	E_x	V_{lJ}
$5/2^+$	2	−3.959	57.73
$3/2^+$	2	−3.859	57.54
$1/2^+$	0	−2.483	53.90
$3/2^-$	1	−0.018	78.588

E. Reaction $^{18}O(n,\gamma)^{19}O$

The ^{19}O nucleus has many states under the $^{18}O + n$ threshold. Most of these states have positive parity. The $5/2^+$ ground state is located at −3.957 MeV. The $3/2^+$ first excited state and $1/2^+$ second excited state are located at −3.861 and −2.485 MeV, respectively. These states are populated by $E1$ capture from the p wave. Two negative-parity states appear: $1/2^-$ at −0.725 MeV and $3/2^-$ at only −0.018 MeV. For the latter state, we adopt the energy of Ref. [7] rather than the usual value −13 keV. Capture from the s wave proceeds mostly to this weakly bound $3/2^-$ state as shown experimentally in Ref. [7]. We thus neglect the capture to the $1/2^-$ state.

The thermal cross section has been measured as 0.16 ± 0.01 mb [7]. Measurements have also been performed at neutron energies between 10 and 80 keV [8] and between 25 and 370 keV [4].

Because several resonances exist below 1 MeV, parametrizing the nonresonant part of the cross sections is more difficult. However, it remains possible by focusing on neutron energies below 300 keV. The potential parameters of reaction $^{18}O(n,\gamma)^{19}O$ are thus chosen to fit the low-energy cross section data to avoid the effect of resonances as much as possible.

The potential parameters we use for reaction $^{18}O(n,\gamma)^{19}O$ are $R = 3.10$ fm and $a = 0.52$ fm. The depths fitting the bound-state energies are given in Table VII. The $s1/2$ depth is also used for scattering in the s wave. The scattering length is 5.75 fm. We have adjusted the depth for the initial p wave. The obtained value is 60 MeV providing a scattering length of −10.2 fm^3.

The various parametrizations are displayed in Table VIII. In our calculations, the spectroscopic factors used for the positive-parity states are taken from the shell model calculation of Ref. [4] and are given in Table VIII. The spectroscopic factor of the $3/2^-$ state is adjusted to the thermal data. The resulting cross section obtained with the potential model is displayed as a solid line in Fig. 4. It reproduces the data below the resonance region. The point at the laboratory energy 370 keV is already affected by the resonance.

TABLE VIII. Same as Table II, but for the reaction $^{18}O(n,\gamma)^{19}O$.

$J_f^{\pi_f}$	l_f	l_i	s_1	s_2	S_0	$\mathcal{S}_{lJ}$
$5/2^+$	2	1	0.0115	−0.075	7.63×10^{-4}	0.69
$3/2^+$	2	1	0.0115	−0.074	4.94×10^{-4}	0.013
$1/2^+$	0	1	−0.233	0.0145	2.36×10^{-3}	0.83
$3/2^-$	1	0	−14.7	1198	4.36×10^{-6}	0.25

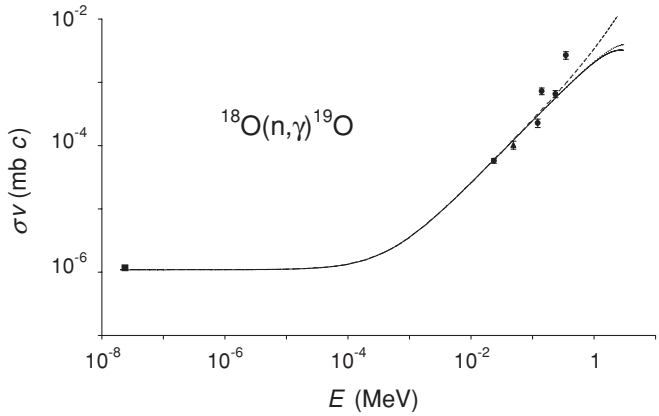

FIG. 4. Comparison of potential model results (full line) and experimental data from Refs. [7] (square), [8] (triangle), and [4] (circles) for the $^{18}O(n,\gamma)^{19}O$ reaction as a function of the neutron c.m. energy in MeV. The dashed and dotted lines represent the Taylor expansion (22) and the Padé expansion (24), respectively.

From Table VIII, the experimental data can be parametrized as

$$\sigma v = 1.09 \times 10^{-6}(1 + 2267E + 836E^2)\,\mathrm{mb}\,c. \qquad (22)$$

Figure 4 shows that the Taylor expansion can fit the potential model well at low energy but has a validity limited to about 30 keV. Beyond that energy, the parametrization of the s-wave partial cross section has a too large slope. This is not surprising: the convergence of the Taylor expansion for s-wave capture is limited as shown by the large s_2 value in Table VIII because of the weakly bound final state at $E_B = -0.018$ MeV. The $E1$ cross section for s-wave capture would be better described with a Laurent series containing a term $(E - E_B)^{-1}$ [31]. Rather than the truncated Taylor expansion (1), we thus propose to use for s-wave capture the Padé-like approximation

$$\sigma v = S_0 \left(1 + s_1 E + \frac{s_2 E^2}{1 - (E/E_B)}\right). \qquad (23)$$

The Taylor expansion of this expression limited at order 2 is still given by Eq. (1); but, in addition, it takes account of the existence of a pole at the bound-state energy E_B.

Combining the Taylor expansions (1) for the various components of p-wave capture with approximation (22) for s-wave capture, one obtains

$$\sigma v = 1.09 \times 10^{-6} \times \left(1 + 2267E - 362E^2 + \frac{1198E^2}{1 + (E/0.018)}\right)\mathrm{mb}\,c. \qquad (24)$$

Expression (24) is easily derived directly from Eq. (22). The coefficient 1198 in the last term is the s_2 value from the $p3/2$ line in Table VIII. The coefficient -362 of the E^2 term is the difference between $s_2 = 836$ in Eq. (22) and 1198. As shown in Fig. 4, this parametrization is valid up to about 0.8 MeV.

IV. CONCLUDING REMARKS

In this paper, nonresonant neutron capture cross sections are parametrized below about 1 MeV by simple polynomials obtained from Taylor expansions. In a case where s wave capture proceeds to a weakly bound state, we have shown that the same Taylor coefficients lead to a much better parametrization under the form of a Padé-like approximation. An exception is $^7Li(n,\gamma)^8Li$, where the domain of validity can nevertheless be enlarged with an empirical modification of the Taylor polynomial. Such approximations can be useful for the interpolation of experimental data and for the measurement of resonance properties.

The derivation of these parametrizations is based on the potential model of neutron capture. It involves a direct calculation of the coefficients of a Taylor expansion on the basis of a plausible potential. The resulting coefficients are weighted by spectroscopic factors and/or by empirical factors fitted on the thermal cross section.

In some cases where $E1$ capture proceeds to positive-parity bound states, we have observed some sensitivity to the scattering length of the initial p wave. Neutron capture may thus offer an indirect way of obtaining some information about the corresponding low-energy phase shifts. Since the value obtained for neutron capture by ^{16}O contradicts a microscopic model [30], it would be interesting to perform a comparison of this model with the same capture data.

Let us emphasize that the present approach can easily be applied to any neutron capture reaction for which the potential model can fairly reproduce the data. This is only possible, of course, in an energy domain without or with few resonances. These parametrizations can also easily be improved if new data become available. The technique can be extended to the microscopic cluster model as will be shown elsewhere.

ACKNOWLEDGMENTS

This text presents research results of the Belgian program P6/23 on interuniversity attraction poles initiated by the Belgian-state Federal Services for Scientific, Technical and Cultural Affairs (FSTC). C.W. thanks Prof. Z.Y. Zhu for providing travel support. He acknowledges the support of the Fund for Scientific Research of Belgium (F.R.S.-FNRS) during his stay in Brussels. O.I.C. thanks the Commission Universitaire de Développement (CUD, Belgium) for supporting his stays in Brussels.

[1] W. L. Imhof, R. G. Johnson, F. J. Vaughn, and M. Walt, Phys. Rev. **114**, 1037 (1959).
[2] Y. Nagai, M. Igashira, N. Mukai, T. Ohsaki, F. Uesawa, K. Takeda, T. Ando, H. Kitazawa, S. Kubono, and T. Fukuda, Astrophys. J. **381**, 444 (1991).
[3] M. Igashira, Y. Nagai, K. Masuda, T. Ohsaki, and H. Kitazawa, Astrophys. J. **441**, L89 (1995).
[4] J. Meissner, H. Schatz, J. Görres, H. Herndl, M. Wiescher, H. Beer, and F. Käppeler, Phys. Rev. C **53**, 459 (1996).

[5] M. Heil, F. Käppeler, M. Wiescher, and A. Mengoni, Astrophys. J. **507**, 997 (1998).
[6] Y. Nagai, M. Igashira, T. Takaoka, T. Kikuchi, T. Shima, A. Tomyo, A. Mengoni, and T. Otsuka, Phys. Rev. C **71**, 055803 (2005).
[7] Y. Nagai, M. Segawa, T. Ohsaki, H. Matsue, and K. Muto, Phys. Rev. C **76**, 051301(R) (2007).
[8] T. Ohsaki, M. Igashira, Y. Nagai, M. Segawa, and K. Muto, Phys. Rev. C **77**, 051303(R) (2008).
[9] M. Igashira, H. Kitazawa, and K. Takaura, Nucl. Phys. **A536**, 285 (1992).
[10] B. J. Allen and R. L. Macklin, Phys. Rev. C **3**, 1737 (1971).
[11] M. Wiescher, R. Steininger, and F. Käppeler, Astrophys. J. **344**, 464 (1989).
[12] R. Reifarth, M. Heil, C. Forssen, U. Besserer, A. Couture, S. Dababneh, L. Dorr, J. Gorres, R. C. Haight, and F. Kappeler *et al.*, Phys. Rev. C **77**, 015804 (2008).
[13] D. Baye, Phys. Rev. C **70**, 015801 (2004).
[14] D. Baye and E. Brainis, Phys. Rev. C **61**, 025801 (2000).
[15] J. E. Lynn, E. T. Jurney, and S. Raman, Phys. Rev. C **44**, 764 (1991).
[16] J. C. Blackmon, A. E. Champagne, J. K. Dickens, J. A. Harvey, M. A. Hofstee, S. Kopecky, D. C. Larson, D. C. Powell, S. Raman, and M. S. Smith, Phys. Rev. C **54**, 383 (1996).
[17] F. C. Barker, Aust. J. Phys. **33**, 177 (1980).
[18] L. Koester, K. Knopf, and W. Waschkowski, Z. Phys. A **312**, 81 (1983).
[19] F. C. Barker, Nucl. Phys. **83**, 418 (1966).
[20] S. Cohen and D. Kurath, Nucl. Phys. **73**, 1 (1965).
[21] S. Cohen and D. Kurath, Nucl. Phys. **A101**, 1 (1967).
[22] N. Kumar, Nucl. Phys. **A225**, 221 (1974).
[23] N. K. Timofeyuk, D. Baye, P. Descouvemont, R. Kamouni, and I. J. Thompson, Phys. Rev. Lett. **96**, 162501 (2006).
[24] T. Nakamura *et al.*, Phys. Rev. C **79**, 035805 (2009).
[25] P. Capel, D. Baye, and V. S. Melezhik, Phys. Rev. C **68**, 014612 (2003).
[26] A. B. McDonald, E. D. Earle, M. A. Lone, F. C. Khanna, and H. C. Lee, Nucl. Phys. **A281**, 325 (1977).
[27] N. Wüst, H. Seyfarth, and L. Aldea, Phys. Rev. C **19**, 1153 (1979).
[28] K. Yamamoto, H. Masui, K. Katō, T. Wada, and M. Ohta, Prog. Theor. Phys. **121**, 375 (2009).
[29] P. Descouvemont and D. Baye, Phys. Rev. C **60**, 015803 (1999).
[30] R. Kamouni and D. Baye, Nucl. Phys. **A791**, 68 (2007).
[31] B. K. Jennings, S. Karataglidis, and T. D. Shoppa, Phys. Rev. C **58**, 579 (1998).